The Journal of Immunology

Formation of a Mast Cell Synapse: Fc{varepsilon}RI Membrane Dynamics upon Binding Mobile or Immobilized Ligands on Surfaces

Amanda Carroll-Portillo, Kathrin Spendier, Janet Pfeiffer, Gary Griffiths, Haitao Li, Keith A. Lidke, Janet M. Oliver, Diane S. Lidke, James L. Thomas, Bridget S. Wilson and Jerilyn A. Timlin

J. Immunol. 2010;184;1328-1338; originally published online Dec 30, 2009;
doi:10.4049/jimmunol.0903071
http://www.jimmunol.org/cgi/content/full/184/3/1328

The Journal of Immunology is published twice each month by The American Association of Immunologists, Inc., 9650 Rockville Pike, Bethesda, MD 20814-3994.

Print ISSN: 0022-1767 Online ISSN: 1550-6606.

Formation of a Mast Cell Synapse: FcεRI Membrane Dynamics upon Binding Mobile or Immobilized Ligands on Surfaces

Amanda Carroll-Portillo,*,† Kathrin Spendier,‡ Janet Pfeiffer,* Gary Griffiths,§ Haitao Li,§,1 Keith A. Lidke,‡ Janet M. Oliver,* Diane S. Lidke,* James L. Thomas,‡ Bridget S. Wilson,* and Jerilyn A. Timlin†

FcεRI on mast cells form a synapse when presented with mobile, bilayer-incorporated Ag. In this study, we show that receptor reorganization within the contacting mast cell membrane is markedly different upon binding of mobile and immobilized ligands. Rat basophilic leukemia mast cells primed with fluorescent anti-DNP IgE were engaged by surfaces presenting either bilayer-incorporated, monovalent DNP-lipid (mobile ligand), or chemically cross-linked, multivalent DNP (immobilized ligand). Total internal reflection fluorescence imaging and electron microscopy methods were used to visualize receptor reorganization at the contact site. The spatial relationships of FcεRI to other cellular components at the synapse, such as actin, cholesterol, and linker for activation of T cells, were also analyzed. Stimulation of mast cells with immobilized polyvalent ligand resulted in typical levels of degranulation. Remarkably, degranulation also followed interaction of mast cells, with bilayers presenting mobile, monovalent ligand. Receptors engaged with mobile ligand coalesce into large, cholesterol-rich clusters that occupy the central portion of the contacting membrane. These data indicate that FcεRI cross-linking is not an obligatory step in triggering mast cell signaling and suggest that dense populations of mobile receptors are capable of initiating low-level degranulation upon ligand recognition. ***The Journal of Immunology*****, 2010, 184: 1328–1338.**

In basophils and mast cells, cross-linking of IgE bound to its cognate high-affinity receptor, FcεRI, triggers release of histamine and other mediators of allergic inflammation. Activated receptors are phosphorylated by Lyn, a membrane-tethered Src-family kinase, on tyrosine residues within ITAM domains of the FcεRI β and γ subunits. Spleen tyrosine kinase (Syk) is subsequently recruited to receptor complexes (1) through interactions of its tandem Src homology 2 domains with ITAMs in the FcεRI γ subunits (2, 3). Syk activation enables propagation of a signaling cascade to downstream components such as linker for activation of T cells (LAT), phospholipase Cγ, and NFAT (4). Signaling is absent in cells lacking Syk (5–7) and delayed in cells lacking Lyn (8), suggesting that other kinases can replace Lyn, albeit inefficiently, and that Syk activation is essential for signaling.

The multisubunit immunorecognition receptor family to which FcεRI belongs also includes the TCR and the BCR. Upon activation by Ag binding, these immunoreceptors also employ Src and Syk family kinases to initiate a phosphorylation cascade for signaling (9–11). Contact between lymphocytes bearing these receptors and either lipid bilayers or APCs bearing ligand leads to formation of an immunological synapse (12–17). Well-known aspects of lymphocyte immune synapses include aggregation of receptor–ligand complexes at the center of the contact site and redistribution of integrins to the periphery. These spatial interactions serve to bridge the two cells and control the responsiveness of signaling.

In this study, we explore the potential for mast cells to form synapses when presented with Ag on surfaces, analogous to the responses of T cells and B cells. Work in the 1980s by the McConnell and McCloskey laboratories (18, 19) established that liposomes bearing haptens for IgE could mediate adhesion to rat basophilic leukemia 2H3 cell line (RBL-2H3) mast cells and provide lateral forces that induced both FcεRI clustering and serotonin release. More recently, Silverman and colleagues (20) described punctate clustering of FcεRI after settling of mast cells on coverslips coated with polyvalent Ag, accompanied by recruitment of Syk and Src homology 2 domain-containing leukocyte protein of 76 kDa. Evidence for direct contacts between mast cells and other immune cells (21–23) indicates that mast cell synapses may play a role in inflammatory responses. In this study,

*Department of Pathology and ‡Department of Physics and Astronomy, University of New Mexico, Albuquerque, NM 87131; †Biofuels and Defense Technologies, Sandia National Laboratories, Albuquerque, NM 87185; and §Imaging Probe Development Center, National Heart, Lung, and Blood Institute, National Institutes of Health, Bethesda, MD 20892

[1]Current address: Division of Chemistry III, Office of Generic Drugs, Center for Drug Evaluation and Research, U.S. Food and Drug Administration, Rockville, MD.

Received for publication September 17, 2009. Accepted for publication November 30, 2009.

This work was supported in part by the Laboratory Directed Research and Development program at Sandia National Laboratories (to J.A.T.), by National Institutes of Health Grant R01AI051575 (to B.S.W.), by the Human Frontiers Science Program (to D.S.L.), by the Army Research Office Grant W911NF0510464 (to K.S.), and by National Institutes of Health Grant P50GM085273 supporting the New Mexico Spatiotemporal Modeling Center. Sandia is a multiprogram laboratory operated by Sandia Corporation, a Lockheed Martin Company, for the U.S. Department of Energy's National Nuclear Security Administration under Contract DE-AC04-94AL85000. The Cancer Center Fluorescence Microscopy Facility received support from National Center for Research Resources Grant 1 S10 RR14668, National Science Foundation Grant MCB9982161, National Center for Research Resources Grant P20 RR11830, National Cancer Institute Grant P30 CA118100, National Center for Research Resources Grant S10 RR016918, the University of New Mexico Health Sciences Center, and the University of New Mexico Cancer Center.

Address correspondence and reprint requests to Dr. Bridget S. Wilson, Department of Pathology and Cancer Center, University of New Mexico Health Sciences Center, Albuquerque, NM 87114 or Dr. Jerilyn Timlin, Sandia National Laboratories, Albuquerque, NM 87185. E-mail addresses: bwilson@salud.unm.edu or jatimli@sandia.gov

The online version of this paper contains supplemental material.

Abbreviations used in this paper: BODIPY-DHPE, *N*-(4,4-difluoro-5,7-dimethyl-4-bora-3a,4a-diaza-*s*-indacene-3-propionyl)-1,2-dihexadecanoyl-*sn*-glycero-3-phospho-ethanolamine, triethylammonium salt; DNP_{24}-BSA, DNP-conjugated BSA; DNP-lysine, Nε-(2,4-DNP)-L-lysine hydrochloride; EGS, ethylene glycol bis(succinimidylsuccinate); FRAP, fluorescence recovery after photobleaching; IgE^{AF488}, Alexa 488-labeled IgE; IgE^{DNP}, anti-DNP IgE; IgE^{Dy520}, Dy520 XL-labeled IgE; LAT, linker for activation of T cells; MβCD, methyl-β-cyclodextrin; POPC, 1-palmitoyl-2-oleoyl-*sn*-glycero-3-phosphocholine; RBL-2H3, rat basophilic leukemia 2H3 cell line; Syk, spleen tyrosine kinase; TEM, transmission electron microscopy; TIRF, total internal reflection fluorescence.

www.jimmunol.org/cgi/doi/10.4049/jimmunol.0903071

transmission electron microscopy (TEM) and total internal reflection fluorescence (TIRF) imaging were combined to more closely examine the spatial relationships of components at the mast cell synapse, including FcεRI, the adaptor LAT, cholesterol, and actin. We show that relationships between these components at the membrane interface differ significantly, depending upon the mobility of ligands on the contact surface. IgE-primed receptors bound to mobile, monovalent ligand form large, centralized, mobile, cholesterol-rich clusters that can initiate weak but measurable signaling (as detected by β-hexosaminidase release) despite the lack of direct cross-linking. Strong signaling to secretion results when IgE–FcεRI complexes are bound to surfaces presenting immobilized, polyvalent ligand. Cholesterol colocalization is markedly lower in the latter case, suggesting that cholesterol trapping does not accompany the immobilization of receptors.

Materials and Methods

Reagents and cell culture

RBL-2H3 and GFP-actin RBL-2H3 cells were maintained in MEM (Invitrogen, Carlsbad, CA) supplemented with 10% FBS, penicillin-streptomycin, and L-glutamine. Affinity-purified anti-DNP IgE (IgE^{DNP}) was prepared as previously described (24, 25). Fluorescent IgE conjugates were created using N-hydroxysuccinimide esters of Alexa 488 (Invitrogen) or Dy520XL (Dyomics, Jena, Germany). Mouse anti-FcεRI β and anti-FITC mAbs were gifts of Dr. Juan Rivera (National Institutes of Health, Bethesda, MD) and Dr. Larry Sklar (University of New Mexico, Albuquerque, NM), respectively. Anti-LAT Abs (Santa Cruz Biotechnology, Santa Cruz, CA) were used in electron microscopy studies, and anti–phospho-LAT Ab (pY191; Epitomics, Burlingame, CA) was used in immunofluorescence.

Exocytosis assay

β-Hexosaminidase release was measured as previously described (26). Briefly, 2×10^5 suspension cells were primed for 2–24 h with 1 μg/ml IgE^{DNP}, then washed and resuspended in HBSS. Primed cells were permitted to settle onto triplicate wells of 24-well plates precoated with mobile or immobile ligands and incubated for 30 min at 37˚C. Supernatants were then collected for degranulation assays. Data are presented as percent of total β-hexosaminidase content released into the medium over 30 min.

Generation and characterization of immobilized/mobile hapten surfaces

Immobilized DNP surfaces. DNP-conjugated BSA (DNP_{24}-BSA at 1 μg/ml; Invitrogen) or Nε-(2,4-DNP)-L-lysine hydrochloride (DNP-lysine at 10 μg/ml; Sigma-Aldrich, St. Louis, MO) were immobilized through cross-linking to poly-L-lysine–coated coverslips or TEM grids with a homobifunctional cross-linker [ethylene glycol bis(succinimidylsuccinate) (EGS); Fisher, Rockford, IL]. Reactions were quenched with 100 mM glycine in PBS, and prepared coverslips were stored in buffer until use.

Mobile surfaces. Liposomes composed of 1.3 mM 1-palmitoyl-2-oleoyl-*sn*-glycero-3-phosphocholine (POPC) and 0–25 mol% *N*-DNP-aminocaproyl phosphatidylethanolamine (Avanti Lipids, Alabaster, AL) were made by hydrating lipid films in PBS and 2 mM Mg^{2+} followed with sonication. Supported lipid bilayers containing DNP-lipid were generated from liposomes on coverslips or electron microscopy grids via liposome fusion at 37˚C and maintained at temperature for experiment duration.

Fluorescence recovery after photobleaching

The mobility of IgE bound to DNP-lipid containing bilayers was measured by fluorescence recovery after photobleaching (FRAP) using a Zeiss LSM 510META confocal microscope with a ×63 1.4 NA oil immersion objective (Zeiss, Thornwood, NY). Bilayers were composed of POPC:N-DNP-aminocaproyl phosphatidylethanolamine with 3 mol% fluorescent lipid *N*-(4,4-difluoro-5,7-dimethyl-4-bora-3a,4a-diaza-*s*-indacene-3-propionyl)-1,2-dihexadecanoyl-*sn*-glycero-3-phospho-ethanolamine, triethylammonium salt (BODIPY-DHPE; Invitrogen). Images were acquired at 400–800 ms/frame using low power 488-nm excitation. A circular region with a 2.5 μm diameter was photobleached by increasing the laser to 95% power for five sequential scans, and recovery was followed. Postbleach curves were fit in MATLAB (The MathWorks, Natick, MD) to estimate the half time and diffusion coefficients according to a linearizing method developed by Yguerabide et al. (27).

FRAP images of the mast cell synapse were acquired on a custom hyperspectral confocal microscope (28) using 488-nm excitation through a ×60 oil-immersion objective (PlanApo VC, NA 1.40; Nikon, Melville, NY) at a rate of 4167 spectra/s. Laser power at the sample was ~100 μW. A 12 μm × 12 μm region encompassing a corner of the synapse and a portion of surrounding area was photobleached by 15 repetitive scans. Recovery scans were taken at 6 and 8 min postbleach. Resulting images were corrected for dark current and offset contributions, and the spectral information from 515–585 nm was binned to produce the final images for recovery analysis.

TIRF imaging

Coverslips with mobile or immobilized ligands were transferred to temperature-controlled chambers (Warner Instruments, Hamden, CT). Cells were prelabeled with Alexa 488-labeled IgE (IgE^{AF488}) or Dy520 XL-labeled IgE (IgE^{Dy520}), allowed to settle onto coated surfaces, and maintained at 37˚C throughout the experiment. Objective-based TIRF imaging was performed as previously described (29) using excitation from a 488-nm continuous wave laser (Model 5450-00C, Ion Laser Technology, Salt Lake City, UT) into an inverted microscope (Olympus IX 71, Olympus America, Center Valley, PA) equipped with an electron multiplied CCD detector (iXon 887, Andor Technologies, Belfast, Northern Ireland) and a ×60 TIRF oil objective (Olympus America) plus ×1.6 magnification in the microscope beam path for a final magnification of ×90. An image splitter (OptoSplit II, Cairn Research, Kent, U.K.) allowed for simultaneous imaging of two spectrally distinct fluorescent labels (AF488, FITC, or GFP in combination with Dy520 XL). Image processing was performed with in-house software implemented in MATLAB (The MathWorks) in conjunction with the image-processing library DIPImage (Delft University of Technology, Delft, The Netherlands).

Epifluoresence and brightfield imaging

To estimate surface binding efficiency, EGS-DNP_{24}-BSA and 25 mol% DNP-lipid bilayers were prepared in eight-well Lab-Tek chambers (Nunc/Thermo Fisher, Rochester, NY). IgE^{DNP}-primed RBL cells (1×10^5) were allowed to settle onto each surface for 12 min at 37˚C. Ten different fields of view were captured using brightfield microscopy with a ×63 1.4 NA oil immersion objective. Average percentage of cells bound to the surface was determined for each surface tested. To evaluate actin and protein reorganization at the synapse, IgE^{AF488}-primed RBL cells in HBSS were settled onto EGS-DNP_{24}-BSA, 25 mol% DNP-lipid bilayers, or bare glass for 6 or 12 min at 37˚C. Samples were fixed using 4% paraformaldehyde and 0.1% Triton X-100 and stained for either rhodamine phalloidin (Invitrogen) or phospho-LAT and FcεRI β. Samples were imaged on an LSM 510META confocal microscope with a ×63 1.4 NA oil immersion objective (Zeiss).

Single particle tracking

IgE^{AF488} on primed cells or bound alone to DNP-lipid–containing bilayers imaged in TIRF was tracked with the ImageJ (National Institutes of Health, Bethesda, MD) SpotTracker plug-in (30) for 15 and 25 s, respectively. The two-dimensional mean squared displacement for various lag times was computed from the extracted particle positions and fit to a line to extract the diffusion coefficient in MATLAB (The MathWorks).

Repletion with fluorescent cholesterol analogs

RBL-2H3 cells were depleted of cholesterol using methyl-β-cyclodextrin (MβCD; Sigma) and then repleted with either FITC-cholesteryl or NBD-6 cholesterol (Avanti Lipids) using a modified protocol optimized for RBL-2H3 cells (31). Briefly, cells were depleted with 10 mM MβCD in media supplemented with 1% fatty acid-free BSA for 30 min followed with repletion using a mixture of unlabeled cholesterol, fluorescent cholesterol, and 5 mM MβCD in media supplemented with fatty acid-free BSA for 30 min. FITC-cholesteryl was synthesized through monoacylation of polyethylene glycol diamine with cholesteryl chloroformate followed by reaction with a fluorescein isothiocyante isomer.

Transmission electron microscopy

Gold grids were coated with formvar and carbon, glow discharged, and treated to present mobile (DNP-lipid bilayers) or immobilized (EGS-DNP_{24}-BSA) ligands. IgE-primed cells were settled onto grids to interact with ligand for designated periods. Samples were then fixed lightly using 0.4%

paraformaldehyde and swollen in a hypotonic buffer (32). Tops of cells were gently blown from the surface with a stream of buffer, leaving behind adherent membrane sheets. Sheets were sequentially labeled with primary Abs and gold-conjugated secondary Abs, stained with tannic acid and uranyl acetate, air dried, and imaged on a Hitachi 7500 TEM (Hitachi, Tokyo, Japan).

Analysis of gold particle distribution and Pearson's coefficient

Digital TEM images were analyzed with an ImageJ plugin customized to find and count coordinates of two sizes of gold particles (National Institutes of Health) (33). Hopkins tests were performed on coordinates to determine if particles were clustered and Ripley's K bivariate function was used to evaluate coclustering (33, 34). Determinations of fluorescence overlap in dual label cholesterol experiments were performed with the ImageJ JACoP plugin (National Institutes of Health; authored by Fabrice P. Cordelieres) for Pearson's coefficient (35).

Results

Surfaces presenting mobile or immobilized DNP

A variety of surfaces were designed to characterize interaction of IgE-primed RBL-2H3 cells with either mobile or immobilized DNP ligand (Fig. 1*A*). Homo-bifunctional cross-linkers were used to covalently attach either DNP_{24}-BSA or DNP-lysine to poly-lysine–coated glass coverslips, generating surfaces presenting immobilized polyvalent or monovalent ligands. Mobile ligand surfaces consisted of bilayers formed from vesicle fusion of DNP-lipid:POPC liposomes. Assuming the area a single phosphocholine occupies is 0.71 nm^2 (36, 37), $\sim 1.4 \times 10^6$ phospholipids would occupy the upper leaflet in a bilayer uniformly covering a square micrometer area surface. By extension, the maximal number of DNP haptens presented to cells by bilayers incorporating 5–25 mol% DNP-lipid would range from $0.7–3.5 \times 10^5$ in the same area. It is possible that this is still a slight overestimate if some amount of DNP is folded into the membrane (19). Importantly, the uniformity of the bilayers was demonstrated using atomic force microscopy (Supplemental Fig. 1), where a 3-nm depth for all bilayers tested was reproducibly measured. Diffusion of lipids in the surface-bound bilayers was confirmed through both single particle tracking and FRAP, as described in *Materials and Methods*. The diffusion coefficients for IgE^{AF488} bound to the DNP-lipid ranged from 0.5–1 $\mu m^2/s$ for bilayers incorporating the lipid at 5 or 25 mol% (Fig. 1*B*). FRAP was performed on bilayers that also included the fluorescent lipid BODIPY-DHPE (3 mol%) in addition to DNP-lipid, demonstrating that recovery of the bleached spot was complete within 0.6 s (Fig. 1*C*). The BODIPY-DHPE exhibited a slightly faster diffusion coefficient (0.9–1.9 $\mu m^2/s$) than DNP-lipid–IgE^{AF488} complexes, potentially explained by the added size of IgE bound to the lipid. As expected, single particle tracking experiments showed that IgE^{AF488} bound to DNP_{24}-BSA remained immobile after EGS-mediated cross-linking to poly-lysine–coated glass surfaces (Fig. 1*B*).

Mast cell synapse develops upon interaction of IgE–FcεRI complex with mobile, monovalent ligand

We next evaluated the dynamics of receptor redistributions upon contact with surface-bound ligands by real-time TIRF imaging of FcεRI primed with IgE^{AF488}. Cells were added to imaging chambers containing coverslips with surface-bound ligands at low enough concentration to avoid confluency. Independent epifluorescent microscopy experiments clarified that >80% of cells added in this manner contacted and adhered to each surface within 12 min. Representative images from TIRF experiments are shown in Fig. 2*A*. Receptor membrane dynamics differed depending on the mobility of the ligand with which they were engaged. Interaction of cells with mobile ligand (DNP-lipid incorporated into a bilayer) over an extended period resulted in formation of a large, centralized region of receptors in the ventral membrane (Fig. 2*A*, *left panels*). As may be seen in Supplemental Video 1 (cluster tracking with the ImageJ

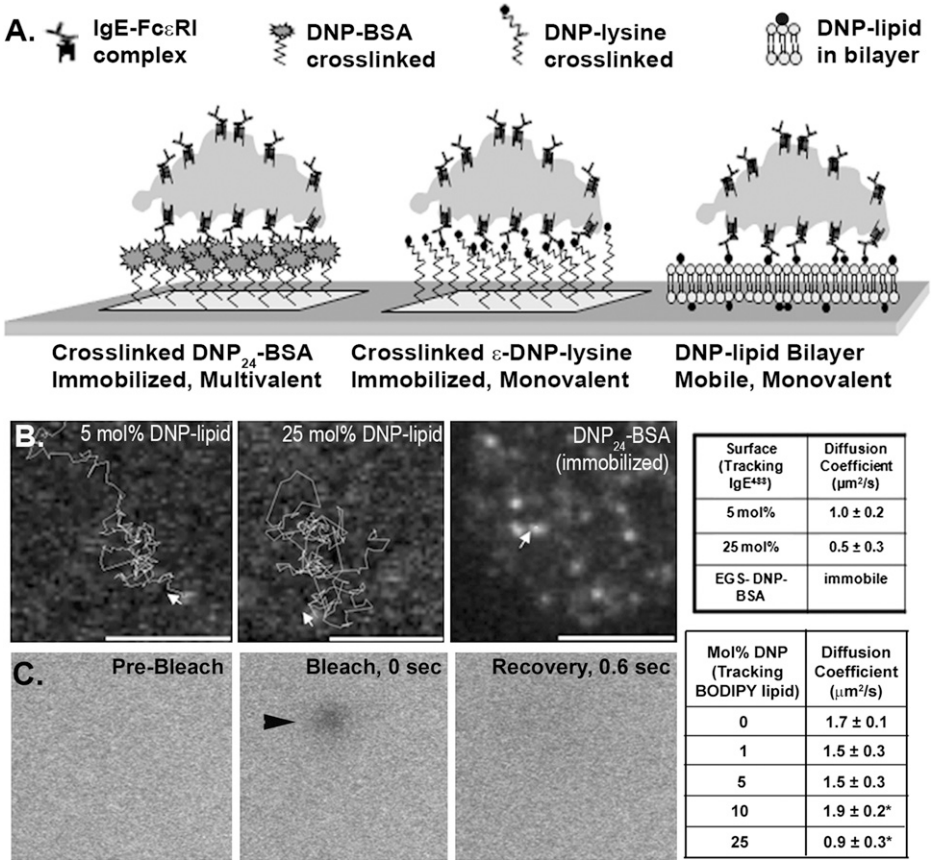

Surface (Tracking IgE^{488})	Diffusion Coefficient ($\mu m^2/s$)
5 mol%	1.0 ± 0.2
25 mol%	0.5 ± 0.3
EGS- DNP-BSA	immobile

Mol% DNP (Tracking BODIPY lipid)	Diffusion Coefficient ($\mu m^2/s$)
0	1.7 ± 0.1
1	1.5 ± 0.3
5	1.5 ± 0.3
10	1.9 ± 0.2*
25	0.9 ± 0.3*

FIGURE 1. Illustration and characterization of surfaces. *A*, Representation of IgE-primed cells contacting different types of Ag-presenting surfaces. *B*, Tracking of fluorescent IgE bound to 5 mol% and 25 mol% DNP-lipid:POPC lipid bilayers and cross-linked DNP-BSA surfaces (original magnification ×150). Arrows indicate starting point and initial direction of each track. Diffusion coefficients were calculated from tracking of IgE^{AF488} bound to each tested surface (table at right). *C*, Sequential images of FRAP performed on a 25 mol% bilayer showing prebleach, bleach spot, and recovery (original magnification ×150). Calculated diffusion coefficients for each surface are indicated in the associated table. *Statistically significant with p value ≤ 0.01; $n = 5$.

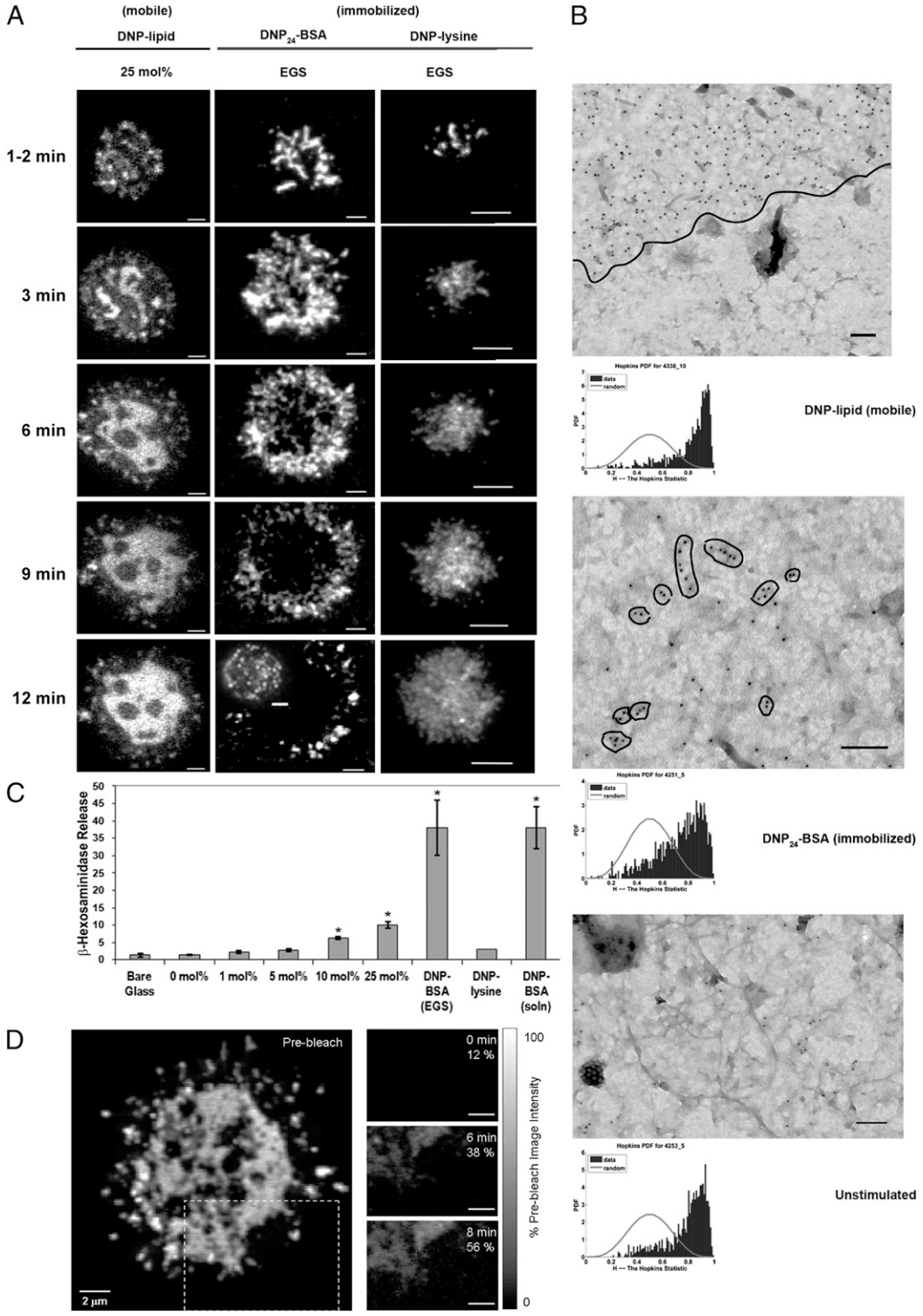

FIGURE 2. Receptor behavior and distribution is dependent upon the type of contact surface. *A*, TIRF imaging of IgE^{AF488}-primed cells engaged with mobile (*left panels*) or immobilized (*middle and right panels*) ligand-presenting surfaces over a 12-min period. Images are contrast enhanced. All scale bars represent 5 μm, original magnification ×90. Disappearance of signal in the central region of the cell settled onto the EGS-DNP-BSA surface is due to photobleaching indicated by another cell imaged under similar conditions without extensive laser exposure (inset image). *B*, TEM images of membrane sheets from cells settled onto mobile (DNP-lipid in bilayer), immobilized (EGS-DNP-BSA) ligand, or nonactivating surface. FcεRI β is labeled with 12-nm or 6-nm gold. Line in *top panel* delineates area of receptor coalescence within the membrane. Hopkins tests are located below each image for which they were performed. Images are contrast enhanced. Scale bars are 100 nm, original magnification ×10,000 (*top panel*) and ×25,000 (*middle* and *bottom* panels). *C*, Percent β-hexosaminadase release from cells settled onto glass, mobile ligand, immobilized ligand, or stimulated by soluble Ag (original magnification ×60). Asterisks indicate results that are significantly higher than spontaneous release (bare glass). *D*, Fluorescence recovery of a bleached portion of a synaptic region formed on a 25 mol% DNP-lipid bilayer. The region outlined in a dashed box indicates region bleached. Bleach and postbleach images taken at 6- and 8-min time points are in the *right panels*. Grayscale range indicator shows amount of fluorescent recovery in each postbleach image. All images were corrected for within-scan photobleaching by scaling to a nonbleached region of the synapse.

Manual Tracking plugin can be seen in Supplemental Fig. 2*B*), the IgE receptors coalesce in the central region of contact with the mobile ligand surface, similar to the behavior of TCR clusters previously reported (38, 39). The appearance and distribution of receptors in contact with DNP_{24}-BSA cross-linked to the surface (immobilized ligand) was markedly different, resulting in rapid formation of stable, moderately sized clusters consistent with diffusional trapping by the immobilized polyvalent ligand (Fig. 2*A*, *middle panels*; Supplemental Video 2). Disappearance of receptor fluorescence on the DNP_{24}-BSA surfaces occurred with repetitive TIRF laser exposure. This was due to photobleaching, as receptor fluorescence could still be detected in cells under the same conditions not exposed to repeated laser illumination (Fig. 2*A*, inset of 12 min DNP_{24}-BSA-EGS panel). Increased photobleaching on the DNP_{24}-BSA surfaces is most likely due to a higher production of reactive oxygen species from this surface as compared with bilayer or DNP-lysine coated surfaces.

To ensure that receptor patterning upon contact with bilayer-incorporated DNP was not due solely to ligand monovalency rather than mobility, receptor morphology was also imaged upon contacting immobilized DNP-lysine (Fig. 2*A*, *right panels*). The immobilized, monovalent ligand neither induced large, coalesced receptor synapses seen with mobile ligand nor the scattered receptor clustering patterns seen with immobilized polyvalent ligand (DNP_{24}-BSA).

Our laboratory has developed gold nanoparticle labeling and TEM imaging of native membrane sheets as a method to evaluate the topographical distributions of receptors and signaling adaptors with nanometer scale resolution (40). The series of TEM images in Fig. 2*B* report receptor distributions on the adherent membranes after IgE-primed cells were allowed to settle on grids coated with mobile (Fig. 2*B*, *top panel*), immobilized ligand (Fig. 2*B*, *middle panel*), or with no ligand (Fig. 2*B*, *bottom panel*). In this procedure, adherent cells were briefly fixed with paraformaldehyde followed by removal of the top of the cell (41, 42). Resulting membrane sheets on grids were fixed and then labeled with immunogold reagents specific for the FcεRI β subunit carboxy terminus (Fig. 2*B*). Typically, by comparison with grids without ligand, grids presenting either mobile or immobilized ligands had increased total numbers of receptors at the adherent surface, presumably due to ligand-mediated capture of receptors diffusing into the region from the remainder of the cell membrane. However, consistent with the TIRF imaging results, the nanoscale patterns of receptor distributions were quite different for each surface examined. On the mobile surface, receptors were found in dense, extensive clusters with a distinct edge (marked with a thin black line in Fig. 2*B*, *top panel*) between the micron-size receptor cluster and neighboring, receptor-free membrane. On the immobilized ligand presenting surface, receptor clusters were more numerous, smaller, and irregularly spaced. Results of the Hopkins spatial statistic test, illustrated by graphs below each TEM image, confirmed that the distribution of receptors is significantly nonrandom under all conditions. The greater right-shift in the Hopkins test for the case of the DNP-lipid (mobile) reflects the larger cluster size under this condition.

Engagement with mobile ligand on lipid bilayers initiates a secretion response

Degranulation assays were performed to characterize β-hexosaminidase release from cells engaged by mobile and immobilized ligand. Results, plotted in Fig. 2*C*, are expressed as a percent of total lysosomal granule β-hexosaminidase content. Interaction of IgE-FcεRI with multivalent, immobilized ligand (DNP_{24}-BSA) resulted in degranulation at levels equivalent to that attained by stimulating cells in solution with DNP_{24}-BSA. Immobilized, monovalent DNP-lysine did not result in β-hexosaminidase release. Remarkably, degranulation was significant after settling of IgE primed mast cells onto 10 or 25 mol% DNP-lipid bilayers where ligand was mobile, monovalent, and not capable of initiating receptor cross-linking.

Receptors within the synaptic region on mobile ligand remain mobile

The rapid photobleaching of receptors trapped on immobilized ligand (Fig. 2*A*, *middle panels*) suggested that imaging of FRAP would be a useful technique to further evaluate overall receptor movements when engaged with mobile ligand at the synaptic surface. Receptor fluorescence at the synaptic region remains dynamic (Supplemental Video 1), making selection of a FRAP region difficult. For this reason, a larger region was selected (Fig. 2*D*, *left panel*, dashed outline) because of its relative flattening and distance from the nucleus. The three images in Fig. 2*D* (*right panels*) report the lack of fluorescence in this area immediately after bleaching, followed by recovery at 6 and 8 min postbleach. Thus, the data demonstrate that receptors engaging mobile ligand at the adherent surface also remain mobile. In support of this conclusion, Table I reports diffusion coefficients derived from experiments tracking IgE^{AF488}-FcεRI receptor clusters (five on each surface) at early time points on immobilized and mobile ligand imaged with TIRF. This table also reports the expected immobility of receptors bound to DNP_{24}-BSA cross-linked to the surface.

Actin reorganization differs on mobile and immobilized ligand surfaces

Actin rings have previously been reported to form at the periphery of the T cell synapse (39, 43). We used GFP-actin–transfected RBL-2H3 cells and rhodamine phalloidin immunofluorescent labeling to evaluate actin reorganization (Fig. 3). TIRF imaging of GFP-actin cells indicated that actin became more concentrated at the cell periphery (ring-like) after cells settled onto surfaces containing mobile ligand (Fig. 3*A*, *middle panels*), despite the lack of integrin binding partners within the bilayer (39). We observed this structural change in >90% of the cells contacting the bilayer. Fixation and staining of cells stimulated with mobile ligand with rhodamine phalloidin resulted in a similar observation (Fig. 3*B*, *top panels*). On immobilized surfaces, an actin network surrounded receptor clusters consistent with previously described actin corrals that restrict receptor movements in unactivated cells (29) (Fig. 3*A*, *bottom panels*). Labeling for rhodamine phalloidin on cells fixed after stimulation with immobilized ligand showed diffuse actin staining throughout the central portion of the contacting membrane (Fig. 3*B*, *bottom panels*) similar to previously reported results (44). Visualization of immunofluorescent labeling was performed using confocal microscopy. TEM images of the corresponding cytoskeleton ultrastructure under each condition are shown in Fig. 3*C*. Taken at relatively low magnification to visualize a larger portion of the membrane sheet, these images showed bundles of cytoskeletal fibers positioned at the edges of membrane adhering to mobile ligands (Fig. 3*C*, *top panel*, boxed region) and an extensive meshwork of fine, filamentous structures on membrane adhering to surfaces presenting immobilized ligand (Fig. 3*C*, *bottom panel*, boxed region).

Table I. *Diffusion coefficients of receptor clusters when bound to mobile or immobilized DNP*

Surface	Diffusion Coefficient ($\mu m^2/s$)
DNP_{24}-BSA (immobilized)	Immobile[a]
25 mol% DNP-lipid (mobile)	$4.1 \times 10^{-3} \pm 1.6 \times 10^{-3}$*
10 mol% DNP-lipid (mobile)	$4.9 \times 10^{-3} \pm 2.1 \times 10^{-3}$*
5 mol% DNP-lipid (mobile)	$9.1 \times 10^{-3} \pm 6.9 \times 10^{-3}$*

[a]Immobile as defined by a diffusion coefficient $<1.0 \times 10^{-5}$ $\mu m^2/s$.
*$p \leq 0.01$. Significant compared with coefficients obtained with DNP_{24}-BSA.

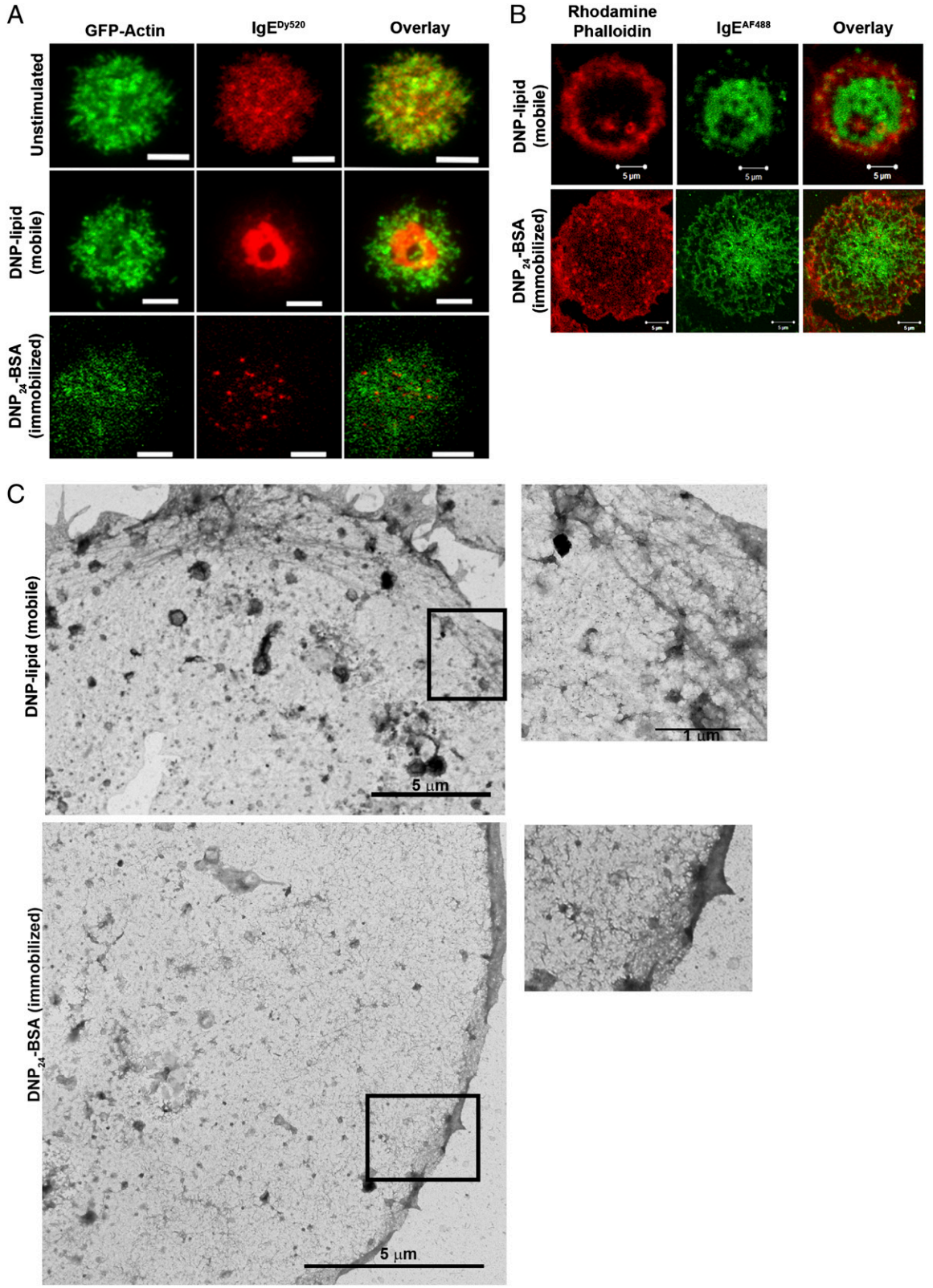

FIGURE 3. Actin reorganization at the adherent surface is dependent upon ligand mobility. *A*, TIRF imaging of GFP-actin RBL-2H3 cells primed with IgE^{Dy520} settled onto glass, mobile (DNP-lipid) ligand, or immobilized (EGS-DNP_{24}-BSA) ligand. Scale bars are 5 μm, original magnification ×90. *B*, Confocal imaging of IgE^{AF488}-primed RBL-2H3 cells fixed with paraformaldehyde and labeled with rhodamine phalloidin. *Top panels* show a cell settled onto a 25 mol% DNP-lipid bilayer, and *bottom panels* show a cell settled onto a DNP_{24}-BSA surface. Scale bars are 5 μm, original magnification ×63. *C*, Low magnification TEM of membrane sheets from cells bound to an bilayer-coated EM grid (*top panel*; original magnification ×1,200, ×12,000, and ×3,500) or a EGS-DNP_{24}-BSA EM grid (*bottom panel*). Magnified views of cytoskeletal structures (boxed regions) for each sheet are in the *right panels*. All images are contrast enhanced.

Cholesterol associates more readily with receptors bound to mobile ligand

Previous work has strongly implicated cholesterol in the integrity and function of receptor clusters (34, 45–48). To study cholesterol dynamics during receptor reorganization upon binding to the two types of surfaces, RBL-2H3 cells were depleted of cholesterol by MβCD treatment and then repleted with a fluorescent cholesterol analog (FITC-cholesterol; illustrated in Fig. 4*A*). In addition to direct imaging of the fluorescent cholesterol, we used anti-FITC Abs combined with TEM and fluorescence-based flow cytometry techniques to: 1) confirm incorporation of the cholesterol derivative into the plasma membrane; and 2) determine the orientation and distribution of FITC-cholesterol in outer and inner leaflets of the lipid bilayer. Table II reports results of a flow

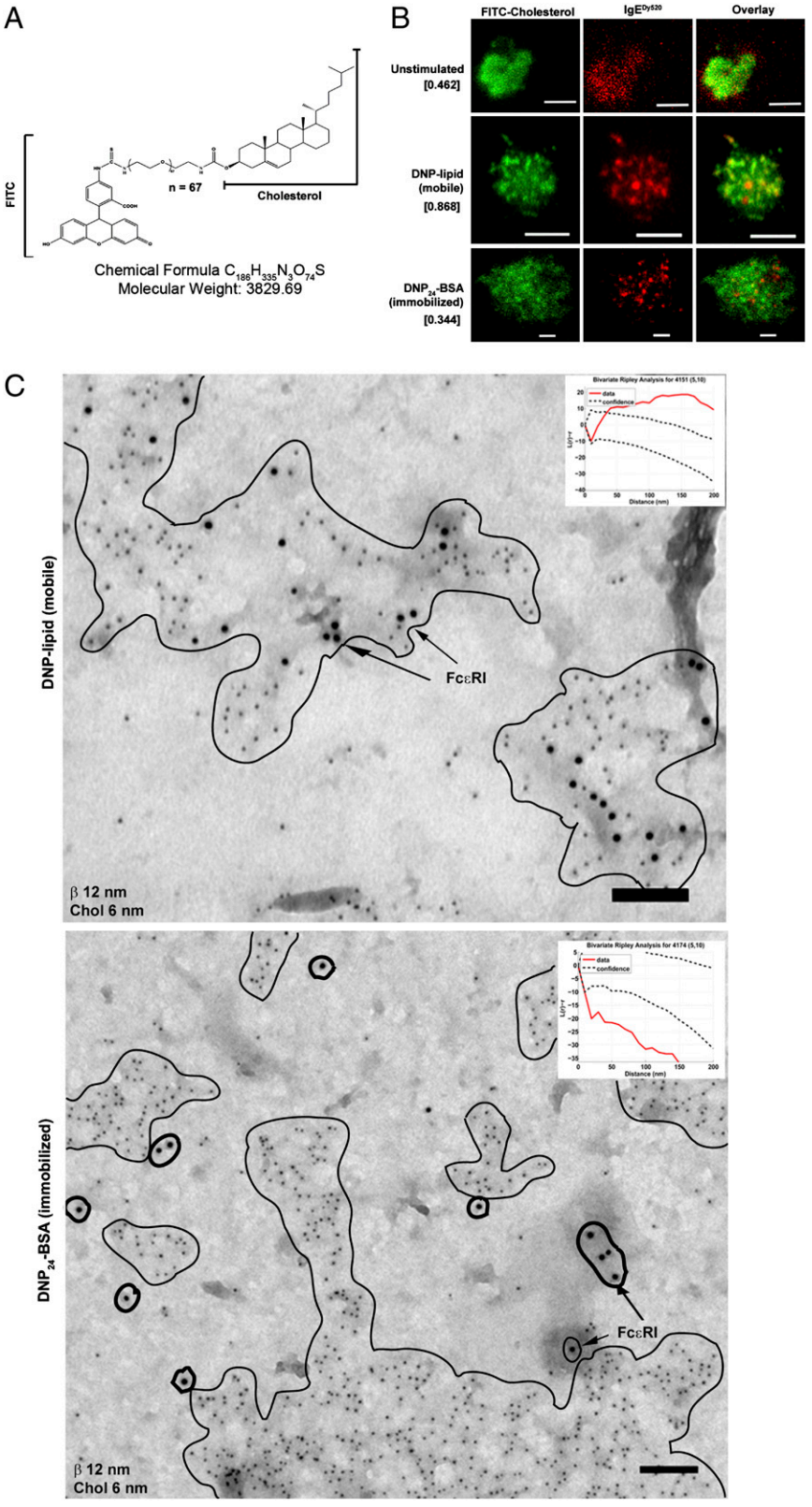

FIGURE 4. Fluorescent cholesterol derivatives reveal strong association with mobile but not immobile FcεRI. *A*, Fluorescent cholesterol analog used in membrane repletion with a short-chain polyethylene glycol linker between the FITC molecule and cholesterol. *B*, TIRF imaging of RBL-2H3 cells repleted with FITC-cholesterol and primed with IgE^{Dy520} after contact with glass (*top panels*), mobile ligand (*middle panels*), or immobilized ligand (*bottom panels*). Pearson's coefficient calculation from each series of fluorescent images is in brackets. Scale bars are 5 μm, original magnification ×90. *C*, TEM membrane sheets from cells settled onto EM grids coated with mobile or immobilized ligand. Regions of receptor (12-nm gold) and cholesterol (6-nm gold) colocalization on the mobile surface are outlined. On the immobilized ligand surface, regions of cholesterol are outlined in a thin line, whereas receptors are circled with a thick line. Ripley's tests for coincidence of label for FcεRI β and FITC (cholesterol) are shown as insets. Scale bars are 100 nm, original magnification ×20,000. All images are contrast enhanced.

Table II. *Quenching of FITC-cholesterol with mAb*

Fluorescent Label	Prequench	Postquench
IgE^{FITC} (2-h labeling)	52.54	9.23
FITC-cholesterol	97.95	36.35

IgE^{FITC}, FITC-labeled IgE.

cytometry-based assay to measure the differences in mean fluorescence intensity for cells loaded for 30 min with FITC-cholesterol, followed with washing alone or washing plus quenching by the addition of anti-FITC mAbs to the extracellular buffer. Quenching of fluorescence of FITC-labeled IgE bound to RBL-2H3 cells served as a control for this assay. The significant loss of fluorescence (>60%) indicates that a large fraction of the FITC-cholesterol resides at least initially in the outer leaflet with the FITC tag extending into the aqueous space, where it is accessible to Abs. Importantly, both live cell and TEM imaging demonstrate the differential association of labeled cholesterol with receptors engaged with either mobile or immobilized ligands. TIRF imaging of RBL-2H3 cells repleted with FITC-cholesterol demonstrated increased overlap of cholesterol-rich regions with receptors when cells contacted mobile ligand (Fig. 4*B*, *middle panels*) as compared with surfaces presenting immobilized ligand. Pearson's coefficient (35) was performed to determine overlap of fluorescent signal from each channel (Fig. 4*B*, bracketed numbers), confirming increased colocalization of cholesterol and receptor complexes on the mobile ligand. In contrast, there was decreased fluorescence overlap between receptors and cholesterol when cells were bound to immobilized ligand (Fig. 4*B*, *bottom panels*). To demonstrate that colocalization was not due to the use of FITC-cholesterol, similar results were obtained in cells repleted with an alternative fluorescent cholesterol analog, NBD-6 cholesterol (Supplemental Fig. 3).

TEM images of membrane sheets from cells stimulated with either immobilized or mobile ligand are consistent with TIRF imaging data (Fig. 4*C*). Membrane sheets were double-labeled with anti-FcεRI β (12 nm) and anti-FITC (6 nm) immunogold reagents. Because Ab was applied after ripping and fixation, and access to the space between the grid and the membrane is limited, we interpret the anti-FITC label as evidence that a portion of FITC-cholesterol has flipped and become incorporated into the inner leaflet of the bilayer. Membrane sheets isolated from cells contacting mobile ligand (Fig. 4*C*, *top panel*) demonstrate the micron-size FcεRI clusters are exceptionally rich in cholesterol; this conclusion is supported by the results of Ripley's bivariate testing (inset) demonstrating labels for the receptor and cholesterol are statistically coclustered. By comparison, there is no significant colocalization between FITC-cholesterol and FcεRI gold labels in membrane sheets prepared from cells activated by immobilized ligand (Fig. 4*C*, *bottom panel*). Ripley's bivariate tests (Fig. 4*C*, insets) confirm these conclusions. The Ripley's bivarate test for the mobile ligand example shows the red data line is well above the confidence interval as proof of strong colocalization. In contrast, for the immobilized ligand example, the red data line falls well below the confidence interval, indicating marked segregation of the two labels within the membrane. The implications of this remarkable difference are discussed below.

LAT segregates from FcεRI clusters in membranes contacting mobile or immobilized ligand

TEM labeling of membrane sheets from RBL-2H3 cells settled onto mobile (DNP-lipid) or immobilized (DNP_{24}-BSA) ligand was performed to evaluate the relative distributions of the protein, LAT, an important adaptor in the FcεRI signaling pathway (Fig. 5). As a dually palmitoylated transmembrane protein, LAT has the characteristics of a raft marker (49). Sheets were double-labeled for FcεRI β (12-nm gold) and LAT (6-nm gold) after settling onto surfaces for 6 min. Counts of LAT label on membrane sheets from mobile (Fig. 5*A*, *top panel*) and immobilized (Fig. 5*A*, *bottom panel*) ligand were performed (data not shown), and the general trend is higher overall number of LAT on membranes isolated from mobile substrates. Membranes from both substrates indicated exclusion of LAT domains from FcεRI clusters, confirmed by Ripley's bivariate testing (Fig. 5*A*, inset graphs, where the red data line falls below the confidence interval). It is interesting to note that, while maintaining a clear segregation, LAT and receptor clusters on surfaces presenting mobile ligand can be close neighbors. This is indicated by the red data line in the Ripley's analysis (Fig. 5*A*, inset graphs), which reverses direction and crosses the confidence interval at a distance in the range of 100–150 nm. These results are consistent with our earlier work labeling membranes for LAT after stimulation with soluble DNP_{24}-BSA (50). To verify that LAT is activated under these conditions, cells were fixed and labeled with anti–phospho-LAT Abs for epifluorescence (Fig. 5*B*). It is worth noting that only the high-resolution TEM imaging can accurately capture the spatial separation between phospho-LAT and FcεRI bound to either immobilized or mobile Ag; this is explained by the resolution of the light microscope being limited to >250 nm, whereas the TEM images revealed proximity of segregated clusters (as close as 100–150 nm).

Discussion

The current paradigm for FcεRI signal initiation requires that IgE-bound receptors be directly cross-linked into aggregates by multivalent ligand. By comparison with Ags with a valency of at least three, soluble dimerizing ligands are often poor at activating FcεRI, although this varies with both spacing of the haptens and overall ligand concentration (51–53). However, early work by McConnell (54, 55) and McClosky (18) showed that vesicles and lipid monolayers bearing monovalent hapten-lipid conjugates could initiate a minimal signal. In this study, we revisit this subject with a combination of high-resolution imaging techniques and show that engagement of IgE-FcεRI with mobile, monovalent hapten at a bilayer interface results in formation of a mast cell synapse that is densely packed with thousands of mobile receptors.

It was demonstrated recently that small, cross-linked FcεRI clusters can remain mobile and signaling competent (51, 56), suggesting that immobilization and large cluster formation are not required for successful signal propagation in response to ligand binding. Remarkably, the results reported in this paper show that monovalent ligand presented in the context of a supported lipid bilayer is also capable of inducing significant degranulation in IgE-primed mast cells, although to a lesser degree than is seen with soluble or immobilized multivalent ligand. There are at least two possible explanations for this observation. The first explanation is that binding of the surface-bound monovalent ligand alone induces a force that promotes a conformational change in the receptor, permitting recruitment of cytoplasmic signaling partners (Lyn, Syk) to the FcεRI cytoplasmic tails. More likely, signaling results because diffusion-mediated trapping at the synapse results in such high density of mobile receptors. In this scenario, there are sufficient collisions between neighboring receptors to promote transient oligomerization and transphosphorylation of FcεRI ITAMS by Lyn. We favor the latter hypothesis, because binding of receptors to immobilized monovalent haptens on surfaces should also exert significant force and yet this method failed to result in

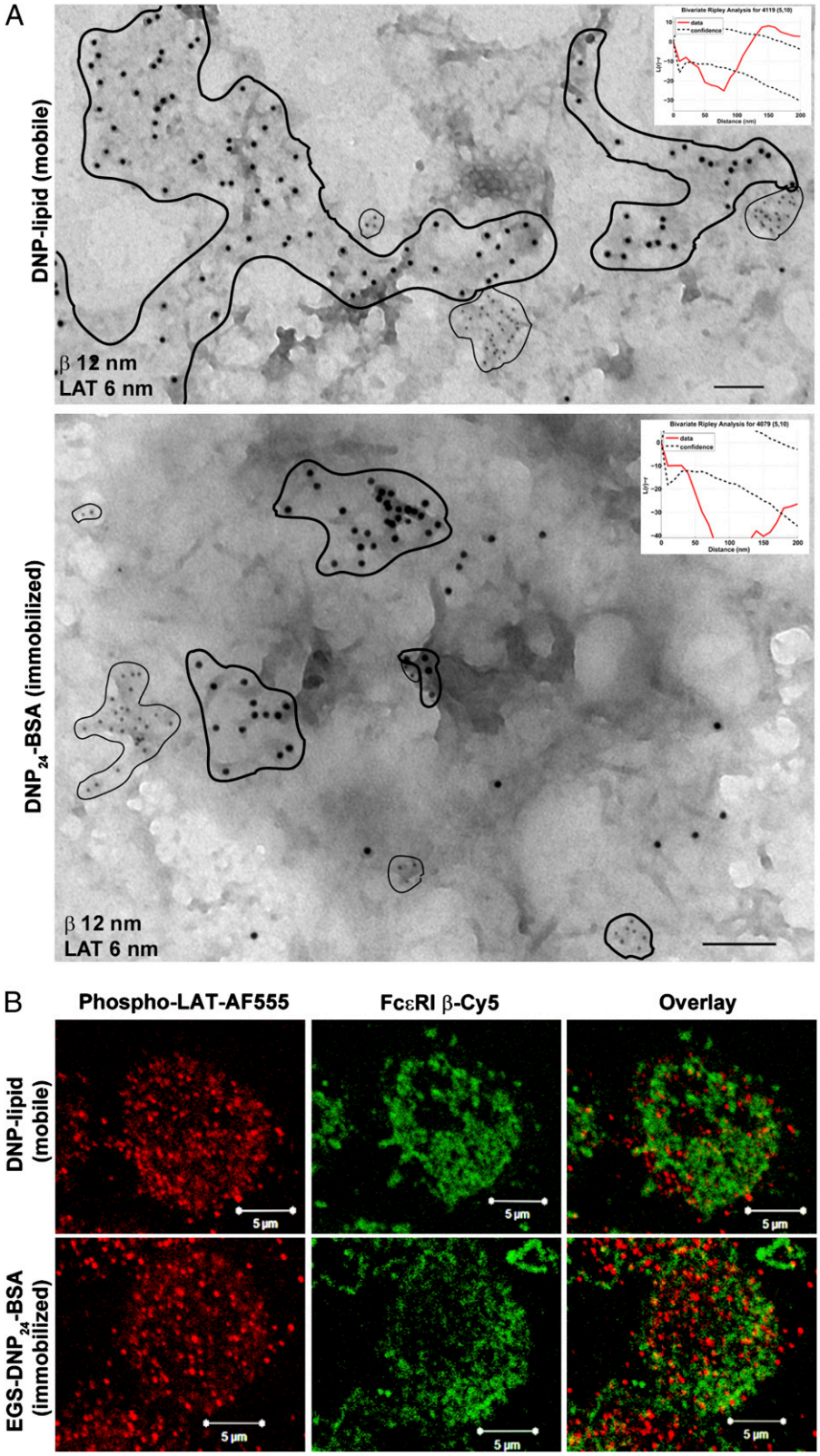

FIGURE 5. LAT clusters do not colocalize with FcεRI at the synapse. *A*, Membrane sheets from IgE primed cells settled onto mobile (*top panel*) or immobilized (*bottom panel*) ligand for 6 min and labeled for FcεRI β (12-nm gold) or LAT (6-nm gold). LAT clusters are circled with thin lines on each sheet to indicate general cluster size and location relative to receptors (circled with thick lines). Scale bars are 100 nm, original magnification ×20,000. Ripley's tests for coincidence of LAT and FcεRI β label are inset in each figure. *B*, Paraformaldehyde-fixed IgE^{DNP}-primed RBL-2H3 cells settled onto 25 mol % DNP-lipid (*top panels*) or DNP_{24}-BSA (*bottom panels*) surfaces for 6 min (original magnification ×63). After permeabilization, cells were dually labeled for phosphorylated LAT (AF555) and FcεRI β (Cy5; psuedocolored). All images are contrast enhanced.

mast cell signaling to degranulation (Fig. 1*C*). We note, however, the immobilized, monovalent haptens were likely to be randomly distributed on the substrate with large spatial separation. Thus, it remains possible that the two mechanisms work in tandem. Because conformational changes have been implicated in triggering signaling by other ITAM-bearing immunoreceptors (16, 57, 58), further work is needed to definitively resolve this issue.

It has been over a decade since the first descriptions of the immunological synapse between T cells and APCs (59–62), marked by dramatic polarization of T cells and central clusters of TCRs surrounded by a ring of adhesion molecules. Engagement of BCR with Ags on the surface of another cell can also lead to B cell polarization, along with many of the hallmarks of the T cell synapse (63). The immunological synapse field continues to

advance, including new concepts regarding the signal amplification properties provided by the synapse platform and the sustainability of signaling through newly arriving receptors (15, 64). In this study, we show that mast cells are also capable of forming a synapse on lipid bilayers and postulate that this is a fundamental capability of most leukocytes. We report the first electron microscopy images of immunoreceptors in contact with ligand-presenting bilayers, providing high-resolution snapshots of synapse organization. It is notable that mast cells can mobilize a synapse on high densities of mobile lipid alone. In physiological settings, we speculate that activation of integrins accompanies FcεRI stimulus (65), facilitating firm adhesion as it does in T cells (66).

Multiple cellular components have been implicated in synapse organization, including lipid composition (1, 45, 67), the cytoskeleton (43), and cytoplasmic scaffolding proteins (68). The role of cholesterol-rich lipid rafts in cell signaling remains an active field of study (69–72). Early work by Baird, Holowka, and colleagues (34, 45–48) described movement of FcεRI into detergent-resistant membrane domains after cross-linking with soluble polyvalent ligand. Our recent lipidomics study concluded that the lipid environment near large FcεRI aggregates, also cross-linked by soluble ligand, is nearly 50% cholesterol (48). In the present work, we used fluorescent cholesterol analogs (31, 73) to image the relationship of cholesterol-rich domains to IgE receptors in the context of the mast cell synapse. Activation of IgE-primed mast cells with mobile, monovalent ligand results in coalescence of cholesterol and receptors within the synaptic region, a result not seen with immobilized ligand. These data are difficult to interpret in the context of current models of the membrane. For example, if cholesterol is so closely associated with the FcεRI as to form part of its lipid shell, a hypothesis originally proposed by Anderson and Jacobson (74), one would expect it to strongly partition with receptors regardless of how FcεRI activation occurs. Yet, cholesterol only partitions with receptor on the surface presenting the mobile ligand. It seems reasonable to speculate that receptors and cholesterol are instead weakly associated, and the diffusive properties of cholesterol favor their dissociation if the receptor becomes immobilized. This postulate is consistent with the work of Davey and colleagues (75), who noted only transient association of FcεRI aggregates with a fluorescent lipid raft probe.

LAT, a dually palmitoylated protein that serves as a scaffold in the FcεRI signaling cascade, is often considered a raft marker (49). We previously showed that LAT clusters enlarge in size after FcεRI activation with soluble polyvalent ligand but segregate strongly from FcεRI clusters (34, 76, 77). Given the remarkable association between cholesterol and FcεRI engaged with mobile ligand at synapse, we also evaluated the potential for greater colocalization between FcεRI and LAT under these conditions. Data presented in Fig. 5, which show that LAT clusters still segregate from the densely packed FcεRI, cholesterol-rich domains at the mobile synapse, suggest that LAT clusters are not equivalent to cholesterol rafts.

Actin reorganization also contributes to formation of the immunological synapse and TCR localization (43). Similar cytoskeletal structural changes occur when mast cells contact mobile ligand to form a synapse (Fig. 3). When mast cells are primed with a heterogenous IgE population (anti-dansyl and anti-DNP) and settled onto mobile ligand (DNP-lipid), IgE–FcεRI complexes that do not recognize the bilayer-incorporated hapten are selectively excluded from the synaptic region (data not shown). This indicates an active selection process for receptor incorporation into the synapse rather than a generalized membrane flow. It is possible that the cytoskeleton and its associated proteins may be involved in this process, a hypothesis that will require further investigation.

This report presents the first detailed characterization of the mast cell synapse. Spatial organization and signaling competency are clearly distinct when receptors are engaged with mobile or immobilized ligands on surfaces. This work sets the stage to explore roles for membrane reorganization when mast cells engage in direct contact with other immune cells. Given recent evidence for mast cells as bona fide immune modulatory cells (21–23), synapses between mast cells and other leukocytes are likely to have functional consequences during immune responses.

Acknowledgments

Confocal images in this paper were generated in the University of New Mexico Cancer Center Fluorescence Microscopy Facility. We thank Ryan Davis for his assistance with hyperspectral confocal imaging, Shannon Coffeil and Nalini Shenoy for preparation of fluorescent cholesterol analogs, and Alan Burns for his contributions to the initial funding of this project. We thank Dr. Gabriel Montano at the Center for Integrated NanoTechnologies, Los Alamos National Laboratories, for performing the atomic force microscopy in the supplemental section.

Disclosures

The authors have no financial conflicts of interest.

References

1. Oliver, J. M., J. R. Pfeiffer, Z. Surviladze, S. L. Steinberg, K. Leiderman, M. L. Sanders, C. Wofsy, J. Zhang, H. Fan, N. Andrews, et al. 2004. Membrane receptor mapping: the membrane topography of Fc(ε)RI signaling. *Subcell. Biochem.* 37: 3–34.
2. Sada, K., J. Zhang, and R. P. Siraganian. 2001. SH2 domain-mediated targeting, but not localization, of Syk in the plasma membrane is critical for FcepsilonRI signaling. *Blood* 97: 1352–1359.
3. Zhang, J., M. L. Billingsley, R. L. Kincaid, and R. P. Siraganian. 2000. Phosphorylation of Syk activation loop tyrosines is essential for Syk function. An in vivo study using a specific anti-Syk activation loop phosphotyrosine antibody. *J. Biol. Chem.* 275: 35442–35447.
4. Gilfillan, A. M., and J. Rivera. 2009. The tyrosine kinase network regulating mast cell activation. *Immunol. Rev.* 228: 149–169.
5. Oliver, J. M., D. L. Burg, B. S. Wilson, J. L. McLaughlin, and R. L. Geahlen. 1994. Inhibition of mast cell Fc ε R1-mediated signaling and effector function by the Syk-selective inhibitor, piceatannol. *J. Biol. Chem.* 269: 29697–29703.
6. Turner, M., E. Schweighoffer, F. Colucci, J. P. Di Santo, and V. L. Tybulewicz. 2000. Tyrosine kinase SYK: essential functions for immunoreceptor signalling. *Immunol. Today* 21: 148–154.
7. Zhang, J., E. H. Berenstein, R. L. Evans, and R. P. Siraganian. 1996. Transfection of Syk protein tyrosine kinase reconstitutes high affinity IgE receptor-mediated degranulation in a Syk-negative variant of rat basophilic leukemia RBL-2H3 cells. *J. Exp. Med.* 184: 71–79.
8. Hernandez-Hansen, V., A. J. Smith, Z. Surviladze, A. Chigaev, T. Mazel, J. Kalesnikoff, C. A. Lowell, G. Krystal, L. A. Sklar, B. S. Wilson, and J. M. Oliver. 2004. Dysregulated FcepsilonRI signaling and altered Fyn and SHIP activities in Lyn-deficient mast cells. *J. Immunol.* 173: 100–112.
9. Depoil, D., M. Weber, B. Treanor, S. J. Fleire, Y. R. Carrasco, N. E. Harwood, and F. D. Batista. 2009. Early events of B cell activation by antigen. *Sci. Signal.* 2: pt1.
10. Geahlen, R. L. 2009. Syk and pTyr'd: Signaling through the B cell antigen receptor. *Biochim. Biophys. Acta* 1793: 1115–1127.
11. Smith-Garvin, J. E., G. A. Koretzky, and M. S. Jordan. 2009. T cell activation. *Annu. Rev. Immunol.* 27: 591–619.
12. Cairo, C. W., R. Mirchev, and D. E. Golan. 2006. Cytoskeletal regulation couples LFA-1 conformational changes to receptor lateral mobility and clustering. *Immunity* 25: 297–308.
13. Dustin, M. L. 2005. A dynamic view of the immunological synapse. *Semin. Immunol.* 17: 400–410.
14. Groves, J. T., and M. L. Dustin. 2003. Supported planar bilayers in studies on immune cell adhesion and communication. *J. Immunol. Methods* 278: 19–32.
15. Huppa, J. B., and M. M. Davis. 2003. T-cell-antigen recognition and the immunological synapse. *Nat. Rev. Immunol.* 3: 973–983.
16. Tolar, P., J. Hanna, P. D. Krueger, and S. K. Pierce. 2009. The constant region of the membrane immunoglobulin mediates B cell-receptor clustering and signaling in response to membrane antigens. *Immunity* 30: 44–55.
17. Tolar, P., H. W. Sohn, and S. K. Pierce. 2008. Viewing the antigen-induced initiation of B-cell activation in living cells. *Immunol. Rev.* 221: 64–76.
18. McCloskey, M. A., and M. M. Poo. 1986. Contact-induced redistribution of specific membrane components: local accumulation and development of adhesion. *J. Cell Biol.* 102: 2185–2196.
19. McConnell, H. M., T. H. Watts, R. M. Weis, and A. A. Brian. 1986. Supported planar membranes in studies of cell-cell recognition in the immune system. *Biochim. Biophys. Acta* 864: 95–106.

20. Silverman, M. A., J. Shoag, J. Wu, and G. A. Koretzky. 2006. Disruption of SLP-76 interaction with Gads inhibits dynamic clustering of SLP-76 and FcepsilonRI signaling in mast cells. *Mol. Cell. Biol.* 26: 1826–1838.
21. Perrigoue, J. G., S. A. Saenz, M. C. Siracusa, E. J. Allenspach, B. C. Taylor, P. R. Giacomin, M. G. Nair, Y. Du, C. Zaph, N. van Rooijen, et al. 2009. MHC class II-dependent basophil-CD4+ T cell interactions promote T(H)2 cytokine-dependent immunity. *Nat. Immunol.* 10: 697–705.
22. Sokol, C. L., N. Q. Chu, S. Yu, S. A. Nish, T. M. Laufer, and R. Medzhitov. 2009. Basophils function as antigen-presenting cells for an allergen-induced T helper type 2 response. *Nat. Immunol.* 10: 713–720.
23. Yoshimoto, T., K. Yasuda, H. Tanaka, M. Nakahira, Y. Imai, Y. Fujimori, and K. Nakanishi. 2009. Basophils contribute to T(H)2-IgE responses in vivo via IL-4 production and presentation of peptide-MHC class II complexes to CD4+ T cells. *Nat. Immunol.* 10: 706–712.
24. Liu, F. T., J. W. Bohn, E. L. Ferry, H. Yamamoto, C. A. Molinaro, L. A. Sherman, N. R. Klinman, and D. H. Katz. 1980. Monoclonal dinitrophenyl-specific murine IgE antibody: preparation, isolation, and characterization. *J. Immunol.* 124: 2728–2737.
25. Seagrave, J., J. R. Pfeiffer, C. Wofsy, and J. M. Oliver. 1991. Relationship of IgE receptor topography to secretion in RBL-2H3 mast cells. *J. Cell. Physiol.* 148: 139–151.
26. Smith, A. J., J. R. Pfeiffer, J. Zhang, A. M. Martinez, G. M. Griffiths, and B. S. Wilson. 2003. Microtubule-dependent transport of secretory vesicles in RBL-2H3 cells. *Traffic* 4: 302–312.
27. Yguerabide, J., J. A. Schmidt, and E. E. Yguerabide. 1982. Lateral mobility in membranes as detected by fluorescence recovery after photobleaching. *Biophys. J.* 40: 69–75.
28. Sinclair, M. B., D. M. Haaland, J. A. Timlin, and H. D. Jones. 2006. Hyperspectral confocal microscope. *Appl. Opt.* 45: 6283–6291.
29. Andrews, N. L., K. A. Lidke, J. R. Pfeiffer, A. R. Burns, B. S. Wilson, J. M. Oliver, and D. S. Lidke. 2008. Actin restricts FcepsilonRI diffusion and facilitates antigen-induced receptor immobilization. *Nat. Cell Biol.* 10: 955–963.
30. Sage, D., F. R. Neumann, F. Hediger, S. M. Gasser, and M. Unser. 2005. Automatic tracking of individual fluorescence particles: application to the study of chromosome dynamics. *IEEE Trans. Image Process.* 14: 1372–1383.
31. Sato, S. B., K. Ishii, A. Makino, K. Iwabuchi, A. Yamaji-Hasegawa, Y. Senoh, I. Nagaoka, H. Sakuraba, and T. Kobayashi. 2004. Distribution and transport of cholesterol-rich membrane domains monitored by a membrane-impermeant fluorescent polyethylene glycol-derivatized cholesterol. *J. Biol. Chem.* 279: 23790–23796.
32. Sanan, D. A., and R. G. Anderson. 1991. Simultaneous visualization of LDL receptor distribution and clathrin lattices on membranes torn from the upper surface of cultured cells. *J. Histochem. Cytochem.* 39: 1017–1024.
33. Zhang, J., K. Leiderman, J. R. Pfeiffer, B. S. Wilson, J. M. Oliver, and S. L. Steinberg. 2006. Characterizing the topography of membrane receptors and signaling molecules from spatial patterns obtained using nanometer-scale electron-dense probes and electron microscopy. *Micron* 37: 14–34.
34. Wilson, B. S., S. L. Steinberg, K. Liederman, J. R. Pfeiffer, Z. Surviladze, J. Zhang, L. E. Samelson, L. H. Yang, P. G. Kotula, and J. M. Oliver. 2004. Markers for detergent-resistant lipid rafts occupy distinct and dynamic domains in native membranes. *Mol. Biol. Cell* 15: 2580–2592.
35. Manders, E. M., J. Stap, G. J. Brakenhoff, R. van Driel, and J. A. Aten. 1992. Dynamics of three-dimensional replication patterns during the S-phase, analysed by double labelling of DNA and confocal microscopy. *J. Cell Sci.* 103: 857–862.
36. Petrache, H. I., S. W. Dodd, and M. F. Brown. 2000. Area per lipid and acyl length distributions in fluid phosphatidylcholines determined by (2)H NMR spectroscopy. *Biophys. J.* 79: 3172–3192.
37. Higgins, M. J., M. Polcik, T. Fukuma, J. E. Sader, Y. Nakayama, and S. P. Jarvis. 2006. Structured water layers adjacent to biological membranes. *Biophys. J.* 91: 2532–2542.
38. Campi, G., R. Varma, and M. L. Dustin. 2005. Actin and agonist MHC-peptide complex-dependent T cell receptor microclusters as scaffolds for signaling. *J. Exp. Med.* 202: 1031–1036.
39. Kaizuka, Y., A. D. Douglass, R. Varma, M. L. Dustin, and R. D. Vale. 2007. Mechanisms for segregating T cell receptor and adhesion molecules during immunological synapse formation in Jurkat T cells. *Proc. Natl. Acad. Sci. USA* 104: 20296–20301.
40. Wilson, B. S., J. R. Pfeiffer, M. A. Raymond-Stintz, D. Lidke, N. Andrews, J. Zhang, W. Yin, S. Steinberg, and J. M. Oliver. 2008. Exploring membrane domains using native membrane sheets and transmission electron microscopy. In *Methods in Molecular Biology: Lipid Rafts*. T. McIntosh, ed. Humana Press, Totowa, NJ, p. 245–261.
41. Avnur, Z., and B. Geiger. 1981. Substrate-attached membranes of cultured cells isolation and characterization of ventral cell membranes and the associated cytoskeleton. *J. Mol. Biol.* 153: 361–379.
42. Pfeiffer, J. R., and J. M. Oliver. 1994. Tyrosine kinase-dependent assembly of actin plaques linking Fc ε R1 cross-linking to increased cell substrate adhesion in RBL-2H3 tumor mast cells. *J. Immunol.* 152: 270–279.
43. Dustin, M. L., and J. A. Cooper. 2000. The immunological synapse and the actin cytoskeleton: molecular hardware for T cell signaling. *Nat. Immunol.* 1: 23–29.
44. Psatha, M., A. Koffer, M. Erent, S. E. Moss, and S. Bolsover. 2004. Calmodulin spatial dynamics in RBL-2H3 mast cells. *Cell Calcium* 36: 51–59.
45. Davey, A. M., R. P. Walvick, Y. Liu, A. A. Heikal, and E. D. Sheets. 2007. Membrane order and molecular dynamics associated with IgE receptor cross-linking in mast cells. *Biophys. J.* 92: 343–355.
46. Pyenta, P. S., D. Holowka, and B. Baird. 2001. Cross-correlation analysis of inner-leaflet-anchored green fluorescent protein co-redistributed with IgE receptors and outer leaflet lipid raft components. *Biophys. J.* 80: 2120–2132.
47. Stauffer, T. P., and T. Meyer. 1997. Compartmentalized IgE receptor-mediated signal transduction in living cells. *J. Cell Biol.* 139: 1447–1454.
48. Surviladze, Z., K. A. Harrison, R. C. Murphy, and B. S. Wilson. 2007. FcepsilonRI and Thy-1 domains have unique protein and lipid compositions. *J. Lipid Res.* 48: 1325–1335.
49. Zhang, W., R. P. Trible, and L. E. Samelson. 1998. LAT palmitoylation: its essential role in membrane microdomain targeting and tyrosine phosphorylation during T cell activation. *Immunity* 9: 239–246.
50. Wilson, B. S., J. R. Pfeiffer, Z. Surviladze, E. A. Gaudet, and J. M. Oliver. 2001. High resolution mapping of mast cell membranes reveals primary and secondary domains of Fc(ε)RI and LAT. *J. Cell Biol.* 154: 645–658.
51. Andrews, N. L., J. R. Pfeiffer, A. M. Martinez, D. M. Haaland, R. W. Davis, T. Kawakami, J. M. Oliver, B. S. Wilson, and D. S. Lidke. 2009. Small, mobile FcepsilonRI receptor aggregates are signaling competent. *Immunity* 31: 469–479.
52. Posner, R. G., D. Geng, S. Haymore, J. Bogert, I. Pecht, A. Licht, and P. B. Savage. 2007. Trivalent antigens for degranulation of mast cells. *Org. Lett.* 9: 3551–3554.
53. Sil, D., J. B. Lee, D. Luo, D. Holowka, and B. Baird. 2007. Trivalent ligands with rigid DNA spacers reveal structural requirements for IgE receptor signaling in RBL mast cells. *ACS Chem. Biol.* 2: 674–684.
54. Cooper, A. D., K. Balakrishnan, and H. M. McConnell. 1981. Mobile haptens in liposomes stimulate serotonin release by rat basophil leukemia cells in the presence of specific immunoglobulin E. *J. Biol. Chem.* 256: 9379–9381.
55. Weis, R. M., K. Balakrishnan, B. A. Smith, and H. M. McConnell. 1982. Stimulation of fluorescence in a small contact region between rat basophil leukemia cells and planar lipid membrane targets by coherent evanescent radiation. *J. Biol. Chem.* 257: 6440–6445.
56. Grodzki, A. C., K. D. Moon, E. H. Berenstein, and R. P. Siraganian. 2009. FcepsilonRI-induced activation by low antigen concentrations results in nuclear signals in the absence of degranulation. *Mol. Immunol.* 46: 2539–2547.
57. Gil, D., W. W. Schamel, M. Montoya, F. Sánchez-Madrid, and B. Alarcón. 2002. Recruitment of Nck by CD3 ε reveals a ligand-induced conformational change essential for T cell receptor signaling and synapse formation. *Cell* 109: 901–912.
58. Ma, Z., P. A. Janmey, and T. H. Finkel. 2008. The receptor deformation model of TCR triggering. *FASEB J.* 22: 1002–1008.
59. Grakoui, A., S. K. Bromley, C. Sumen, M. M. Davis, A. S. Shaw, P. M. Allen, and M. L. Dustin. 1999. The immunological synapse: a molecular machine controlling T cell activation. *Science* 285: 221–227.
60. Monks, C. R., B. A. Freiberg, H. Kupfer, N. Sciaky, and A. Kupfer. 1998. Three-dimensional segregation of supramolecular activation clusters in T cells. *Nature* 395: 82–86.
61. Shaw, A. S., and M. L. Dustin. 1997. Making the T cell receptor go the distance: a topological view of T cell activation. *Immunity* 6: 361–369.
62. Wülfing, C., and M. M. Davis. 1998. A receptor/cytoskeletal movement triggered by costimulation during T cell activation. *Science* 282: 2266–2269.
63. Batista, F. D., D. Iber, and M. S. Neuberger. 2001. B cells acquire antigen from target cells after synapse formation. *Nature* 411: 489–494.
64. Dustin, M. L. 2008. T-cell activation through immunological synapses and kinapses. *Immunol. Rev.* 221: 77–89.
65. Kepley, C. L., L. Youssef, R. P. Andrews, B. S. Wilson, and J. M. Oliver. 2000. Multiple defects in Fc ε RI signaling in Syk-deficient nonreleaser basophils and IL-3-induced recovery of Syk expression and secretion. *J. Immunol.* 165: 5913–5920.
66. Sims, T. N., and M. L. Dustin. 2002. The immunological synapse: integrins take the stage. *Immunol. Rev.* 186: 100–117.
67. Holowka, D., J. A. Gosse, A. T. Hammond, X. Han, P. Sengupta, N. L. Smith, A. Wagenknecht-Wiesner, M. Wu, R. M. Young, and B. Baird. 2005. Lipid segregation and IgE receptor signaling: a decade of progress. *Biochim. Biophys. Acta* 1746: 252–259.
68. Shaw, A. S., and E. L. Filbert. 2009. Scaffold proteins and immune-cell signalling. *Nat. Rev. Immunol.* 9: 47–56.
69. Jacobson, K., O. G. Mouritsen, and R. G. Anderson. 2007. Lipid rafts: at a crossroad between cell biology and physics. *Nat. Cell Biol.* 9: 7–14.
70. Mondal, M., B. Mesmin, S. Mukherjee, and F. R. Maxfield. 2009. Sterols are mainly in the cytoplasmic leaflet of the plasma membrane and the endocytic recycling compartment in CHO cells. *Mol. Biol. Cell* 20: 581–588.
71. Shaikh, S. R., and M. A. Edidin. 2006. Membranes are not just rafts. *Chem. Phys. Lipids* 144: 1–3.
72. Hancock, J. F. 2006. Lipid rafts: contentious only from simplistic standpoints. *Nat. Rev. Mol. Cell Biol.* 7: 456–462.
73. Shaw, J. E., R. F. Epand, R. M. Epand, Z. Li, R. Bittman, and C. M. Yip. 2006. Correlated fluorescence-atomic force microscopy of membrane domains: structure of fluorescence probes determines lipid localization. *Biophys. J.* 90: 2170–2178.
74. Anderson, R. G., and K. Jacobson. 2002. A role for lipid shells in targeting proteins to caveolae, rafts, and other lipid domains. *Science* 296: 1821–1825.
75. Davey, A. M., K. M. Krise, E. D. Sheets, and A. A. Heikal. 2008. Molecular perspective of antigen-mediated mast cell signaling. *J. Biol. Chem.* 283: 7117–7127.
76. Lebduska, P., J. Korb, M. Tůmová, P. Heneberg, and P. Dráber. 2007. Topography of signaling molecules as detected by electron microscopy on plasma membrane sheets isolated from non-adherent mast cells. *J. Immunol. Methods* 328: 139–151.
77. Wilson, B. S., J. R. Pfeiffer, and J. M. Oliver. 2002. FcepsilonRI signaling observed from the inside of the mast cell membrane. *Mol. Immunol.* 38: 1259–1268.